

# Chapter 7

## Evaluation of Artificial Hearts



**B. Y. Su and L. P. Chua**

**Abstract** Due to the shortage of heart donors, ventricular assist device (VAD) has been developed as a temporal or permanent cardiac support. Essentially, a continuous flow VAD is a rotary pump to maintain blood supply. In addition to hydraulic efficiency and output power, the blood damage induced by a VAD must be minimized to mitigate potential complications. It has been found in the literature that the blood damage is closely related to detailed flow field, which could only be visualized by experimental measurements and computational fluid dynamic (CFD) simulations. During the development of a VAD, CFD is widely used for optimization, and several numerical models have been proposed to estimate blood damage level. In this chapter, we demonstrated a typical study of an axial flow VAD. The physical model included a straightener, an impeller, and a diffuser, and several designs of diffuser were numerically modeled for optimization in terms of hydraulic and hemodynamic performances. To validate numerical results, experimental measurements at different regions were conducted using particle image velocimetry (PIV). It is worth noting that similar procedure would be applied to a centrifugal blood pump. Before clinical application, animal and clinical trials must be conducted to examine its actual blood damage level and other potential issues, which are valuable for next iteration of design if needed.

**Keywords** Computational fluid dynamics · Artificial hearts · Hemodynamics

---

B. Y. Su  
National Heart Research Institute Singapore, National Heart Centre Singapore, Singapore, Singapore

L. P. Chua (✉)  
School of Mechanical and Aerospace Engineering, Nanyang Technological University, Singapore, Singapore  
e-mail: [mlpchua@ntu.edu.sg](mailto:mlpchua@ntu.edu.sg)

## 7.1 Introduction

Due to the modern hectic and unhealthy life style, such as obesity and lack of exercise, there are more people engaging heart disease than before. Some of them may lead to even heart failure and required heart transplant as a last mean to keep them alive. However, the available heart donors are always lacking far behind the demand of the healthy hearts over the world. Luckily with the advance of technology, artificial heart pumps are invented and improved over the time as an alternate mean to help these heart failure patients. Mechanical circulatory support devices can be categorized into total artificial heart (TAH) and ventricular assist device (VAD), and the latter is more widely implanted than the former, especially at the left ventricle (i.e., LVAD). The VAD has been considered as a useful therapeutic modality for bridge-to-transplantation, bridge-to-recover, or even long-term cardiac support [1, 2]. Nevertheless, either one of these two devices (LVAD and RVAD) can be used to bridge across the semilunar valve by connecting the inlet to the ventricular device directly so as to provide energy to eject the blood. On the other hand, the inlet cannulation of left VAD can be placed at the apex with the outlet connected back to aorta, and the inlet of right VAD is located at the superior vena cava with blood ejected to the left pulmonary arteries through outlet. In general, the continuous flow VADs are based on the spinning of a rotor to provide the required energy, that is why they are being named as rotary pumps, with the two most used types are centrifugal and axial pumps. The centrifugal pump has a much bigger size than the axial pump. Centrifugal flow pumps are suitable to generate higher pressure and lower flow rates, whereas axial flow pumps are usually used to generate lower pressure and higher flow rates [3]. The axial pump has also much higher rotating speed than the centrifugal pump, in the long run, the blood may prefer much lower speed of centrifugal pump, which is closer to the nature of the blood flow, but more data is required to prove it. Besides the conventional hydraulic design, the hematologic design has to be considered due to the blood is the fluid being used. Although up to now, the real physiological mechanism of hemolysis and thrombosis processes is not fully known, the scientists are interpreting them from the physics point of view. The hemolysis is due to the shearing effects, it is then connected to the shear stress and the duration of exposure time using the power law, while the formation of thrombus is fluid mechanics related e.g., the stagnation flow, recirculation, and flow separation. Therefore, these phenomena should be minimized or even eliminated if possible, besides the more complicated physiological and biological factors. During optimization phase, computational fluid dynamics (CFD) is a popular tool to numerically estimate both hydraulic and hemodynamic performances before the much expensive prototype fabrication and testing. After the CFD simulation, the experimental validation is necessary, and there are many techniques available such as flow visualization (FV), Laser Doppler anemometer (LDA), and particle image velocimetry (PIV). Each technique has its advantages and limitations. A standard hemolysis test is now used to measure the damage of blood caused by the artificial heart pumps such as the axial and centrifugal pumps for the animal trial, and the

Normalized Index of Hemolysis (NIH) for example is one of the few parameters to indicate the level of blood damage.

## 7.2 Pulsatile or Non-pulsatile Circulation

In nature the human heart can be treated as a pulsatile pump, and the blood being ejected will flow in both pressure and volumetric waveforms. It is then created a fundamental question to the scientists to answer whether it is a must to keep the arterial pulsation in order to maintain enough blood flow and aerobic metabolism for all the essential organs. Since most artificial hearts are basically miniature rotary pumps, pulsatile circulation indicates the necessity of varying rotating speed during cardiac cycle. In contrast, constant rotating speed can only produce non-pulsatile circulation.

A relatively large amount of study has been carried out in connection with the hemodynamic effects on the pulsatile versus non-pulsatile circulation in animals including human being. The pulsatile perfusion creates advantage on peripheral organs, which is very likely mediated by its effect on systemic vascular resistance and the microcirculation. The pulsation improves splanchnic perfusion and plays an essential role in the movement of lymph in and out of the intestine, the prevention of edema, and the maintenance of capillary patency through the prevention of sludging. The brain microcirculation and cerebrospinal fluid movement are shown to be improved with pulsation, which was also found to improve aerobic tissue metabolism.

Wesolowski et al. [4] have challenged the necessity of maintaining pulsatile circulation in 1953 and successfully kept the circulation and normal organ function for a brief period using non-pulsatile blood flow. The continuous flow implantable DeBakey VAD device has been adopted by Potapov et al. [5] to detect the flow in peripheral vessels and measured transactional Doppler signals in patients after implantation. They [5] have shown that patients with severe heart failure can maintain their lives with the continuous flow VAD. The use of DeBakey VAD resulted in normal organ function and provides unloading of the left ventricle, which can lead to partially restore myocardial function. It has been shown that despite the non-pulsatile flow produced by DeBakey VAD, the pressure changed due to contractions of unloaded left ventricle and the partially recovered right ventricle provided a nearby physiological pulsatile flow. The first clinical experience with the DeBakey VAD is positive and leads to its continuous use. Statistical data indicates that DeBakey VAD has supported over 200 patients at 14 different heart centers and in 7 countries around the world [5]. The mean flow rate for these trials ranged from 3.6 to 5.0 L/min, and cerebral blood flow and, furthermore, organ function were maintained with few signs of hemolysis and thrombosis [6]. Garatti et al. [7] compared the pre- and post-transplant outcomes between pulsatile and non-pulsatile flow VADs and they concluded that the continuous flow pumps were as effective on bridging to transplantation rates, mortalities, and post-transplant

incidences of treated rejections when compared to pulsatile pumps. Although there is no clear conclusion, non-pulsatile circulation has been widely employed in the clinical setting of cardiopulmonary bypass or circulatory support [8]. In terms of design of artificial heart, it is acceptable to set certain constant rotating speed that can generate enough pressure head and flow rate.

## **7.3 Blood Trauma**

### **7.3.1 Hemolysis**

Hemolysis is defined as the breakdown or destruction of red blood cells (RBCs), and the released hemoglobin (Hb) may activate platelet activation and coagulation cascade. Therefore, the continuous lysing or destruction of RBC can weaken its ability to transport oxygen. An obvious pinkish color can be found in the serum due to hemoglobin, when only a small amount of 0.5% of RBCs are being destroyed. This has enhanced the chance to cause renal failure since an excess of plasma-free hemoglobin is toxic [9]. The use of artificial heart pump on patients has inevitably enhanced the chances of physical contact between the blood and solid pump surfaces of the device, which will cause mechanically RBCs rupture, even the applications of artificial heart valves and the hemodialysis treatment as well as the usage of the heart-lung support machine during, for example, bypass operation will have the similar effects and results [10]. Minimal blood damage is therefore an important pre-requisite and demand of artificial heart and even valve devices. Hemolysis is an essential and sensitive indicator of blood trauma, and in vitro assessment provides valuable parameters and feedback for optimization of VAD design features such as blood contact surface finish, pump blade shape, and blood flowing clearance during prototype development. It is therefore very important to be able to predict the mechanical hemolysis which can be concluded to be a very critical parameter and issue for the design and application of VADs.

### **7.3.2 Thrombus**

The final product of the blood coagulation step is blood clot and is named as a thrombus, which is very essential and important to predict thrombus formation for designing and finally production of any medical devices with blood flow. Compared with hemolysis, the mechanism of thrombus formation is much more complicated and there are many complicated processes to induce thrombus in blood flow [11]. Whenever there is a damage of blood vessel, platelets and von Willebrand Factor (vWF) will stick to the wall. After platelets react with collagen, fibrinogens react with them under the proper shear rate and clots are generated by platelet, vWF,

and fibrinogen. These aggregations are called thrombus *in vivo*. In artificial organs, especially rotary VADs, these aggregations can be found at wall and other parts.

It was observed in animal studies that the shear rates of 1300–1700 (1/s) and 300 (1/s) might be corresponding to the white and red thrombus formation thresholds, respectively, and Yamane et al. [13] have proposed the following two mechanisms: (1) In the case of white thrombus or platelet aggregation, platelets are thought to be activated by high shear rate flow and to deposit on surfaces with low shear rate; (2) In the case of red thrombus or fibrin gel capturing RBCs, it can be argued that low shear rate simply induces coagulation of RBCs. In the development of various types of cardiac prostheses, Nose [12] had experienced that (1) during the first 2 weeks of postoperative period, the white thrombus likely forms inside the implanted prosthesis, and (2) after 2 weeks, all the blood contacting surfaces are pacified by proper protein so that white thrombus is more likely not to form inside for a long period of time. Kihara et al. [15] found that the usage of the anticoagulation coating, for example, 2-methacryloyloxyethyl phosphorylcholine (MPC) polymer, can slow down the platelet adhesion, complement activation, and protein absorption, and consequently they have concluded that it is very efficient in reducing the thrombus formation.

It is found that the conditions of local blood flow can greatly affect the shape, structure, and size of thrombus. The endothelial damage may be caused by the higher shear flows, and further triggers pathological platelet clumping to the vessel wall. On the other hand, platelet aggregates with low levels of granule released from platelets or RBC response can be activated by low shear stress levels. Additionally, interactions between platelets and RBCs, platelets and platelets, or even RBCs and RBCs with a regional stagnant flow can also induce thrombus formation. Further, Ramstack et al. [16] showed that the integrity of the fibrin clot is affected by the local shear flow. It is also found by Hashimoto et al. [13] that thrombus formed easily when blood was subjected to low shear rate of less than 500 (1/s). Furthermore, Wurzinger et al. [18] showed that a low shear flow results from recirculation and vortices, which trap the cells leading to an increase in the local wall shear stress [14]. Moreover, abrupt cross-sectional widening of flow regions may produce flow separation and potentially secondary flow, creating circumstances favorable for thrombus formation.

## 7.4 Evaluation

### 7.4.1 *In Vitro Measurement of Hemolysis*

Hemolysis test has now been taken as a routine and standard method in the evaluation of hemolysis parameters *in vitro* study of rotary VADs. A schematic view of a hemolysis test arrangement conducted by Arvand et al. [15] is shown in Fig. 7.1. A reservoir bag is connected to an artificial heart pump using silicone tubes with pressure indicator and flowmeter mounted to monitor pressure heads and flow

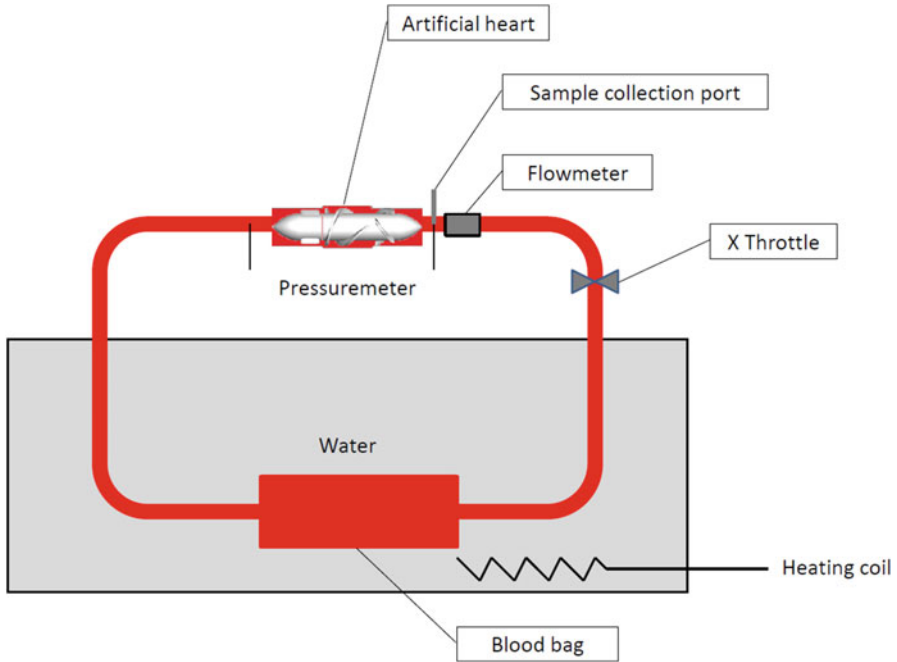


**Fig. 7.1** Experimental arrangements for hemolysis tests [15]

rates of the pump, respectively. Fresh bovine blood, goat blood, or even human blood can be tested, and the reservoir bag is submerged in a warmed water bath with temperature kept constant at about 37 °C. Pressure across the pump can be adjusted using resistance throttle applied over a 10 cm length tube to minimize potential for hemolysis due to local narrowing of the tube. After the circuit is filled with the blood suspension, all visible air bubbles should be vented from the blood sampling port and no air interface remained in the reservoir. During the hemolysis test, blood aliquots are sampled from the circulating blood at a regular time interval, and the plasma concentration of hemoglobin is measured thereafter for each sample.

To evaluate blood damage from medical devices such as VADs with continuous blood flow, ASTM F1841-97 Standard [16] proposes three relations for the laboratory measurement of the damage to erythrocytes: NIH, the Normalized milligram Index of Hemolysis (mgNIH), and the Modified Index of Hemolysis (MIH). The NIH and mgNIH measure the increase in plasma-free hemoglobin in grams and milligrams per 100 L of pumped blood, respectively. The MIH, normalized by the total quantity of the hemoglobin in the volume within the closed circuit of the pump device, in a closed circuit, is used to measure the increase in plasma-free hemoglobin. The MIH is the chosen engineer measurement presentation due to it is dimensionless [9].

$$\text{NIH(g/100L)} = \Delta\text{freeHb} \times V \times \frac{100 - \text{Ht}}{100} \times \frac{10^2}{Q \times T} \quad (7.1)$$

$$\text{MIH} = \frac{\Delta\text{freeHb}}{\text{Hb}} \times V \times \frac{100 - \text{Ht}}{100} \times \frac{10^6}{Q \times T} \quad (7.2)$$

where  $\Delta\text{freeHb}$  (L/min) is the increase in plasma-free hemoglobin concentration (g/L) over the time interval,  $V$  is the circuit volume (L),  $\text{Ht}$  is the hematocrit (%),  $Q$  is the flow rate (L/min), and  $T$  is the sampling time interval (min).

There are quite a number of different and controversial criteria for the cell rupture in the literatures. The mechanism of hemolysis is not fully understood; however, the following three factors listed below are generally believed that the threshold for cell lysis could be affected;

1. Measurement method. Grigioni et al. [17] commented that the orientation of the measurement system affects the shear stress being obtained, when using three-dimensional Laser Doppler Anemometer (LDA) as a measuring tool.
2. Nature of either laminar or turbulent flow. Wurzinger et al. [18] used viscometer to measure hemolysis at laminar shear stress up to 255 Pa and exposure times of 700 ms, while Sallam and Hwang [19] find out that under turbulent flow, the Reynolds shear stress can be as high as 400 Pa under the corresponding estimated exposure time of 1 ms.
3. Material used in experiment. Paul et al. [11] found that the application of the carbon ring seals has strong effect on the measured hemolysis level, as compared with the result obtained by Wurzinger et al. [18] under comparable conditions.

### 7.4.2 *Animal and Clinical Trials*

Various artificial hearts have been developed during last few decades and some have undergone animal and/or clinical trials. Due to the complexity of blood, the assumptions related to blood damage are not able to accurately estimate its responses to artificial heart pump, and thus it is compulsory to conduct such trials over certain period of time. Impella CardioSystems (Aachen, Germany) has developed a micro-axial VAD with minimal invasive treatment for the purpose of a temporary support of the left ventricle in acute situations [20]. A maximum blood flow of 2.4 L/min with pressure head of 50 mmHg when the integrated motor drives the impeller at the speed of 50,000 rpm is being designed for this pump. Due to its small size, this percutaneous pump is inserted across the aortic valve with the aid of guidewire through the femoral artery and aorta. This pump has applied to ten patients in 2006 during the high-risk percutaneous coronary interventions [21]. It was found that the free hemoglobin level increased above 1, 5, and 10 times the upper limit of the normal one in some patients. It was therefore concluded that the routine use of this device was not encouraged. The MicroMed-DeBakey VAD has been designed in cooperation with NASA/Johnson Space Center, Baylor College of Medicine, and

MicroMed Technology Incorporated. It could provide a flow rate of 5–6 L/min and a pressure of 100 mmHg with the inducer-impeller running at about 10,000 rpm and requires input power less than 10 W. Calves were being operated as animal test in order to estimate the overall performance and hemodynamic effects before the clinical trial in 1999 [22]. Based on the review in 2011, this device is redesigned to reduce high incidence of thromboembolic complications [23]. HeartMate II (Thoratec Inc., Pleasanton, CA) has only one moving part and textured blood contacting surface, and it is 40 mm in diameter with a weight of 176 g. It was FDA approved in 2010 for use as destination therapy for end-stage heart failure and is the most widely implanted VAD with more than 10,000 implants globally [24].

### ***7.4.3 Numerical Evaluation of Artificial Heart***

CFD technique as a design tool has been widely adopted to simulate and analyze fluid flows within and around objects of interest, and it significantly influences the development of artificial hearts [25–27]. CFD has the ability to evaluate design promptly at early stage before the commitment being made on the very expensive prototype manufacturing and testing. At the detailed design stage, CFD can also quickly find out the effects of design changes on blood flow to totally avoid or at least reduce the risk of unexpected knock-on effects that would otherwise become obvious only at a later stage. CFD technique has been widely adopted in the development stage of any blood contacting medical device including heart valves, VADs, stents, grafts, blood access, purification devices, etc. The critical challenge for a VAD design is to combine both the hematologic and hydraulic designs optimally [28]. In particular, designers using traditional methods often do not realize that local high shear stress levels and/or flow stasis have the potential to invalidate a design due to adverse hematologic consequences. The application of CFD technique is the most promising avenue for achieving these optimization tasks [29]. When a final design has been reached, CFD analysis can be used to confirm that design goals have been achieved. Detailed CFD results of flow field can often be used to support and explain experimental results, potentially strengthening regulatory submissions and providing a scientific base for clinical application. Due to the limitations of some measuring techniques which results in some blind spots or region of the flow field cannot be obtained, however, CFD is able to overcome these weaknesses with a much lower cost. The basic architecture and flowchart of a CFD-based design process is demonstrated in Fig. 7.2 [30]. The overall goal of the design process is to systematically evolve from some inferior initial designs to an optimized design. The main modules of the design process include: (1) CFD analysis, (2) design evaluation, (3) design modification, and (4) geometry modification.

In order to reduce the costs of design and development of artificial organs, various numerical approaches have been conducted to quantify the shear-induced hemolysis [31]. From the comparative stress theory of fluids that is analogous to the Mises yield criterion for solid materials, Bludszuweit [36] has developed the scalar shear stress,



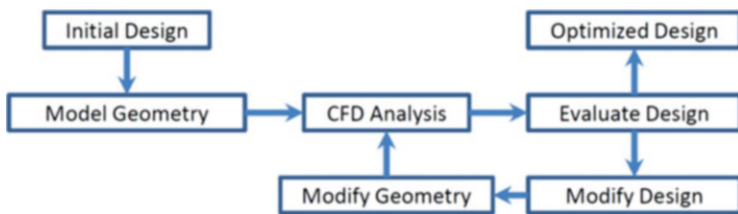


**Fig. 7.2** Flowchart of a CFD-based design

which consists of six components of the stress tensor and represents the level of shear experienced by the blood. The scalar shear stress estimation provides information about regions of high stress levels (possible hemolysis) and extremely low levels (like stasis risking thrombosis). In the present investigation, this approach was adopted to account for the three-dimensional shear field and obtained the scalar shear stress according to the stress formula of Bludszuweit [32] as listed below as Eq. (7.3):

$$\tau = \left[ \frac{1}{3} \left( \tau_{ii}^2 + \tau_{jj}^2 + \tau_{kk}^2 \right) - \frac{1}{3} \left( \tau_{ii}\tau_{jj} + \tau_{jj}\tau_{kk} + \tau_{kk}\tau_{ii} \right) + \left( \tau_{ij}^2 + \tau_{jk}^2 + \tau_{ki}^2 \right) \right]^{1/2} \quad (7.3)$$

$$\tau_{ij} = \sigma_{ij} + \rho \overline{u'_i u'_j}$$

$$\sigma_{ij} = \mu \left( \frac{\partial u_i}{\partial x_j} + \frac{\partial u_j}{\partial x_i} \right)$$

$$\overline{\rho u'_i u'_j} = -\frac{2}{3} \rho k \delta_{ij} + \mu_t \left( \frac{\partial u_i}{\partial x_j} + \frac{\partial u_j}{\partial x_i} \right)$$

where  $\delta_{ij}$  is the Kronecker Delta which equals to 1 for  $i = j$  and 0 for  $i \neq j$ ;  $k$  signifies the turbulent energy term;  $\rho$  is the fluid density;  $u_i$  is the velocity component in  $x_i$  direction;  $u'_i$  is the fluctuating part of the velocity; and  $\mu$  and  $\mu_t$  are the molecular and turbulent viscosities, respectively.

A simple but effective correlation between shear stress, exposure time, and the extent of damage to erythrocytes by the power law is developed by Giersiepen et al. [33] under the condition of uniform shear stress. The effectiveness of a power-law formulation as a mathematical model of blood trauma is considered to be suitable only in the presence of the predominance of simple laminar flow. However, the power-law equation provides an acceptable prediction for comparison purposes [34].

$$d\text{Hb}/\text{Hb} = 3.62 \times 10^{-7} \times t^{0.785} \times \tau^{2.416} \quad (7.4)$$

where  $d\text{Hb}/\text{Hb}$  is the ratio of plasma-free hemoglobin to total hemoglobin,  $\tau$  is the characteristic scalar shear stress (Pa), and  $t$  is the stress exposure time (s).

There are generally two approaches to apply Eq. (7.4). The most widely used model is based on accumulated blood damage along a particle track or a streamline. A number of particles are released from the inlet of the numerical domain, and the accumulated blood damages along these tracks are averaged at outlet as the estimated hemolysis. The detailed equations and procedure are described in the following paragraphs.

Trace data of particles along a streamline can be collected, and the shear stress induced in each particle can be calculated. It is assumed that the damage index ( $D$ ) associated with each particle has a value of 0 initially when the particle enters into a VAD, and increases monotonically due to accumulation of blood damage along the particle trace. When  $D$  reaches a value of 1, this particle breaks. The equations are described as follows:

$$d_{p,i} = 3.62 \times 10^{-7} \times \tau_i^{2.416} \Delta t_i^{0.785} \quad (7.5)$$

where  $d_{p,i}$  is the blood damage of  $i$ th particle,  $p$ , during time interval,  $\Delta t_i$ , between  $t_i$  and  $t_{i+1}$ .

The damage accumulation from time 0 to  $t_i$  is given by the following:

$$D_{p,i} = D_{p,i-1} + (1 - D_{p,i-1})d_{p,i} \quad (7.6)$$

Hemolysis index ( $E$ ) is defined as the mean damage:

$$E = \frac{1}{N} \sum D_p \quad (7.7)$$

where  $N$  is the total number of particles.

#### 7.4.3.1 Physical Model

Su et al. [29, 35] have done a baseline analysis by means of classic pump design formulas and empirical diagrams to obtain initial pump geometry. As demonstrated in Fig. 7.3, the original design consisted of a three-blade straightener, a two-blade impeller, and a three-blade diffuser. The impeller was shrouded by a cylinder, where the magnet was embedded, and thus both components rotated simultaneously. A 0.2 mm clearance gap was specifically designed for the gap between suspended shroud and pump casing for the present blood pump. The impeller was designed to transfer energy to blood, while the diffuser converted the kinetic energy of the blood from the spinning impeller in circumferential direction to pressure head. For the ease of comparison, the three-blade diffuser (B3) of axial flow blood pump (See Fig. 7.3a) is shown in Fig. 7.3b. The five-blade diffuser (B5) and a three-blade diffuser with a clearance gap of 0.2 mm between the diffuser blades and hub (B3C2) are shown in Fig. 7.3c, d, respectively.

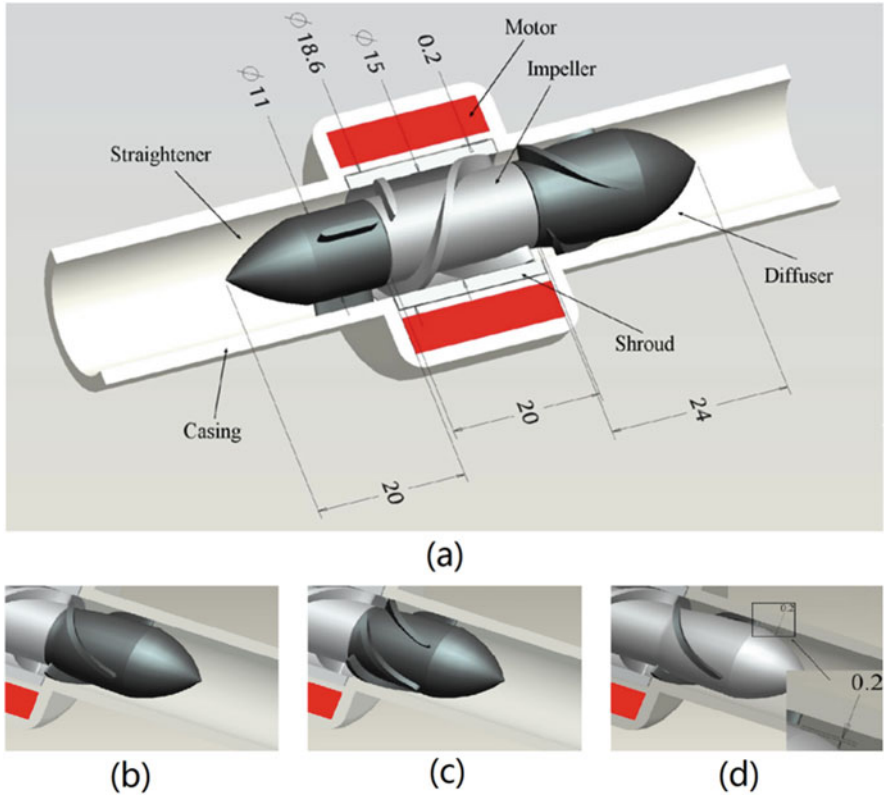


**Fig. 7.3** (a) An axial flow blood pump assembly; (b) the three-blade diffuser (B3); (c) the five-blade diffuser (B5); and (d) the three-blade diffuser with 0.2 mm clearance gap (B3C2). All dimensions in mm. Note that in (b–d) the stationary and rotating hub are indicated by dark and light gray, respectively [29]

**7.4.3.2 Numerical Model**

The blood was assumed as a Newtonian fluid with constant dynamics viscosity of  $3.5 \times 10^{-3}$  Pa s and density of  $1050 \text{ kg/m}^3$ . The designed operating speed was around 10,000 rpm, and the corresponding Reynolds number was more than  $3 \times 10^4$ . Therefore, the internal flow was turbulent, and shear stress transport  $k-\omega$  turbulence model was selected for numerical simulation [29, 36]. Since the structure of the axial flow pump was complex, it was divided into three regions connected with interfaces and meshed separately. Approximately, 1.5 million hexahedral grids were generated after grid dependency test. Simulations were conducted using ANSYS FLUENT as finite-volume method based CFD solver.

### 7.4.3.3 Hydraulic Performance

Pressure-flow curves and hydraulic efficiencies of the three diffuser designs at rotating speed of 10,000 rpm that are based on numerical simulations are shown in Fig. 7.4. Normally, the flow rates of a rotary blood pump for an adult range from 4 to 6 L/min, so all these designs are able to provide adequate static pressure head. The static pressure head drops more steeply in B3C2 model, and the B3 model has the highest static pressure head followed by B5 and B3C2 models at the designed flow rate of 5 L/min. The flow rates at the highest efficiency points are 5–6 L/min, and the hydraulic efficiencies vary between 20% and 26%. The lowest hydraulic efficiency of B3C2 is due to the extra torque required to rotate the diffuser hub.

The velocity vector distributions on the circular sectional slice in the middle between the diffuser hub and tip in different designs are shown in Fig. 7.5. Flow at the diffuser entrance is in the tangential direction following the blade profile smoothly until the region near the trailing edge of side A, where flow separation was observed in Fig. 7.5a, b. It is because of the curvature of the diffuser blade and adverse static pressure gradient along flow direction. Increment of blade number reduced the flow separation region (Fig. 7.5a vs. Fig. 7.5b), which vanished (Fig. 7.5c) due to the rotation of diffuser hub.

### 7.4.3.4 Hemodynamic Performance

The numerical estimation of hemolysis mentioned earlier has been applied to different diffuser designs. Approximately, 1000 path-lines were collected from inlet to outlet, and the time interval of 0.1 ms was adopted. It can be observed in Fig. 7.6 that the indices were affected by both rotating speed and flow rate, further, among the three models, B3C2 has the highest estimated hemolysis index followed by B3 and B5.

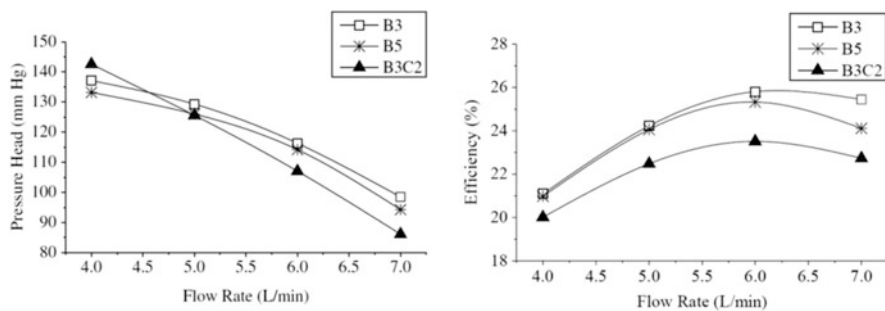


**Fig. 7.4** Pressure-flow curve (left) and efficiency-flow curve (right) predicted by CFD at rotating speed of 10,000 rpm

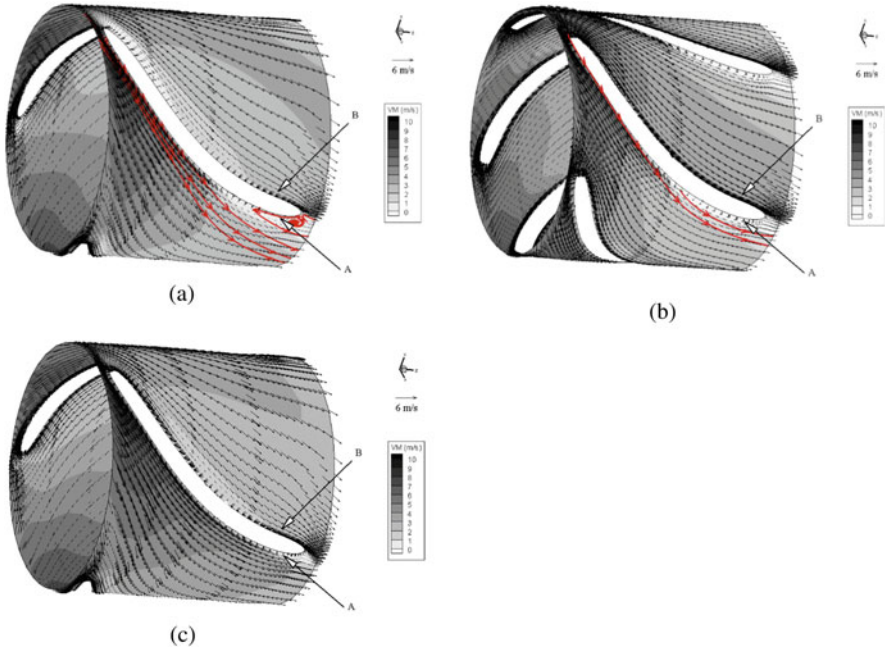


**Fig. 7.5** Velocity vector distributions on circular sectional plane at 5 L/min. (a) B3, (b) B5, and (c) B3C2. Streamlines are illustrated near blade trailing edge to indicate reverse flow

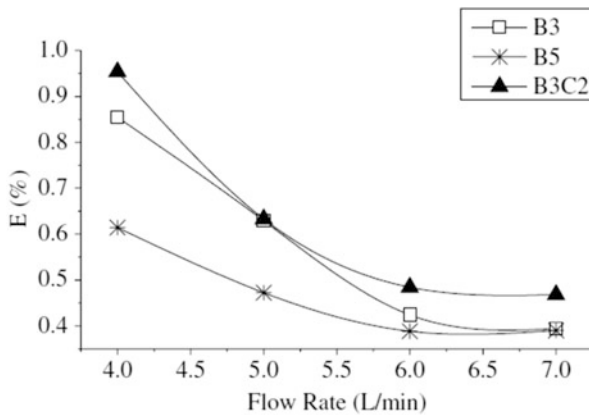


**Fig. 7.6** Estimated hemolysis indices at 10,000 rpm

**7.4.3.5 Comparisons Based on Numerical Results**

Various parameters could be derived from the numerical results, and some are summarized in Table 7.1. For the ease of comparison, linear interpolation was applied to predict these values under the same operating conditions (i.e., 5 L/min and 100 mmHg). As shown in the table, the rotating speeds are 9080, 9130, and

**Table 7.1** Comparison of selected parameters in each design

		$\omega$ (rpm)	$\eta$ (%)		FS		$E$ (%)
B3	+	9080	23.90	–	Yes	0	0.34
B5	0	9130	23.70	0	Yes	+	0.30
B3C2	–	9250	22.00	+	No	–	0.43

Best and worst performances are indicated by a plus and a minus sign, respectively, while 0 represents neutral. Note:  $\omega$  rotating speed,  $\eta$  hydraulic efficiency, FS flow separation,  $E$  estimated hemolysis index

9250 rpm for B3, B5, and B3C2, respectively. Both rotating speed and hydraulic efficiency are related to hydraulic performance, and thus were considered under a single group. Based on the table, B5 was superior to the other two. Generally, this example demonstrates a typical approach of numerical evaluation of artificial heart, which includes design of baseline model and its improvements, mesh generations, selections of turbulence model and blood damage model, and the final analyses and comparisons. Owing to the fast advancement of computational speed and parallel computing, the simulation should be completed in a couple of hours. Compared with the optimization using prototypes, the iteration is much more efficient and faster with better cost-effectiveness.

#### 7.4.4 *Experimental Measurements for Validation*

The pressure-flow curves obtained from in vitro measurements could be used for the validation of the numerical simulation; however, the acquisition of detailed flow field is necessary to examine the competence of selected turbulence model. To visualize flow field, optical access is compulsory, and thus the prototype of artificial heart is transparent. To minimize refraction, the refraction index of blood analog should be close to that of the prototype of artificial heart, which is mostly made of acrylic. The more traditional point-based LDA technique is considered to be the “gold standard” due to its high accuracy and resolution. Since it is able to capture the original fluid fluctuating velocity signal and can be easily used to find the average and root mean square velocities, furthermore these capture turbulence signals can be further processed to obtain for example turbulent kinetic energy, turbulent production rates, and Reynolds stresses. The LDA does not have to calibrate for every measurement, since its signal depends on the specific immutable frequency of laser radiation for direct measurements of velocity. The only disadvantage may be time consuming to acquire the whole flow field using LDA since it is a point-based measurement. This can be overcome by the PIV technique which is able to capture information of the whole flow field in a relatively short time. Beside using seeding particles as the LDA, the PIV measurements make use of high-speed digital camera to capture a successive image pair within a laser-illuminated plane [36]. With the usage of a pulsed laser, each image pair is obtained during a relatively short time interval compared with the transit time of the particle through the measurement

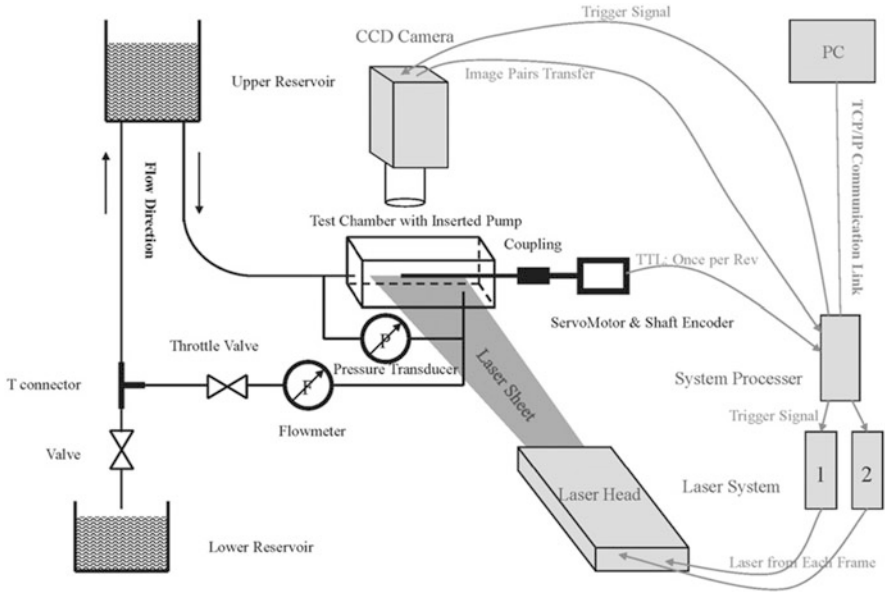


**Fig. 7.7** Schematic view of the experimental test rig

region. With the known time interval, the local velocity in any subregion of these acquired images can be found by comparing the particle displacement between a pair of images. This approach completely maps the instantaneous velocity field within the planar illuminated region. Generally, the frequency that PIV system can achieve is in the order of 10–15 Hz, and it is insufficient to capture the turbulent flow structures that have typical frequencies in the order of 10, 100 Hz, and even higher. In contrast, the sampling frequency of LDA can reach as high as 20 MHz. The other weakness of PIV is that the experimental results are only sufficient to capture the mean velocity but not for higher moment turbulence quantities.

Since the primary purpose of experimental measurement is to validate simulation results, it would be desirable if the optical accessible prototype has the same scale of the numerical model [35, 36]. However, prototypes could be scaled up in some studies by obeying similarity laws [26]. Figure 7.7 shows a typical arrangement of experimental measurement of an axial flow pump using PIV, which was designed by Su et al. [36]. The blood analog was firstly injected into the upper reservoir, and then the test chamber was fully filled through the flexible tubes. When the experiment begins, the flow rate of VAD is controlled by the throttle valve located at the downstream of the flow meter. The flow rate and pressure head across the pump model could be found from the flowmeter and pressure transducer, respectively. For illumination of the laser sheets and image acquisition, the VAD model was made of acrylic, and the impeller was driven by a metal shaft, which was further connected to the servomotor mounted with 3-channel optical shaft encoder.

The Dantec FlowMap PIV system from the Dantec Dynamics A/S, Skovlunde, Denmark, was used in the present study. While the Gemini PIV 200-15 from the New Wave Research, Fremont, CA, USA, a double cavity pulsed neodymium aluminum garnet (Nd:YAG) laser system generated two pulsing beams to form pulsing light sheets, and it was further synchronized to shaft encoder through FlowManager software. During the measurement, the servomotor precisely controlled the impeller, and the “once-per-revolution” signal from the shaft encoder triggered the laser and image acquisition. Therefore, the images were taken at designed angular position of the impeller over 100 revolutions. In order to adjust the angular position, a delay was set between shaft encoder and trigger signal. The captured images were sent to system processor and stored in PC through communication link eventually. The charge-coupled device (CCD) camera used was HiSense MkII camera (Hamamatsu C8484-05 digital CCD chip:  $1280 \times 1024$ ). The measurement area was  $10.76 \times 8.26 \text{ mm}^2$  with the scale factor of 1.25, and the aperture was  $f/5.6\sim 8$ . The interrogation area of  $32 \times 32$  pixels was applied with 50% overlap. The final velocity map was obtained by averaging 100 pairs of images.

A qualitative agreement between the numerical and experimental results could be observed in Fig. 7.8 for flow distributions at (a) straightener, (b) impeller, and (c) diffuser, respectively. Note that the solid line and dotted line denote PIV and CFD results respectively in these figures for quantitative comparison. The discrepancies between the experiment and PIV results, which are relatively obvious, can be found at the regions close to the blades, hub, and inner casing surfaces in the figure, due to a few reasons. The fluid close to the interfaces usually has higher velocity gradient in radial direction, owing to the inhomogeneity of fluid field. According to the principle of PIV, the movements of seeding particles in an interrogation area should be homogeneous to estimate velocity accurately. Secondly, the trapped seeding particles on surface could induce relatively strong reflection, leading to an error in PIV measurements. Generally, the CFD results agree fairly well with the PIV results, especially in the straightener region. The L2 relative error norm of the differences in axial velocity between CFD and PIV with respect to the PIV in the straightener, impeller, and diffuser are 11%, 19%, and 27%, respectively. Note that the L2 relative error norm is defined as  $\sqrt{\sum_{i=1}^N (f_i^E - f_i^N)^2 / \sum_{i=1}^N (f_i^E)^2}$ , where  $f_i^E$  and  $f_i^N$  represent the values from node  $i = 1$  to  $i = N$  for PIV experiment and numerical simulation, respectively.

## 7.5 Summary

Due to the shortage of heart donors, artificial heart becomes a feasible approach to support patients with end-stage heart failure. Alternatively, it is used as a temporal solution to maintain blood circulation. Mostly, the essential part of artificial heart is a blood pump to generate adequate pressure head and flow rate. However, the blood damage must be carefully managed and minimized to avoid medical complications.



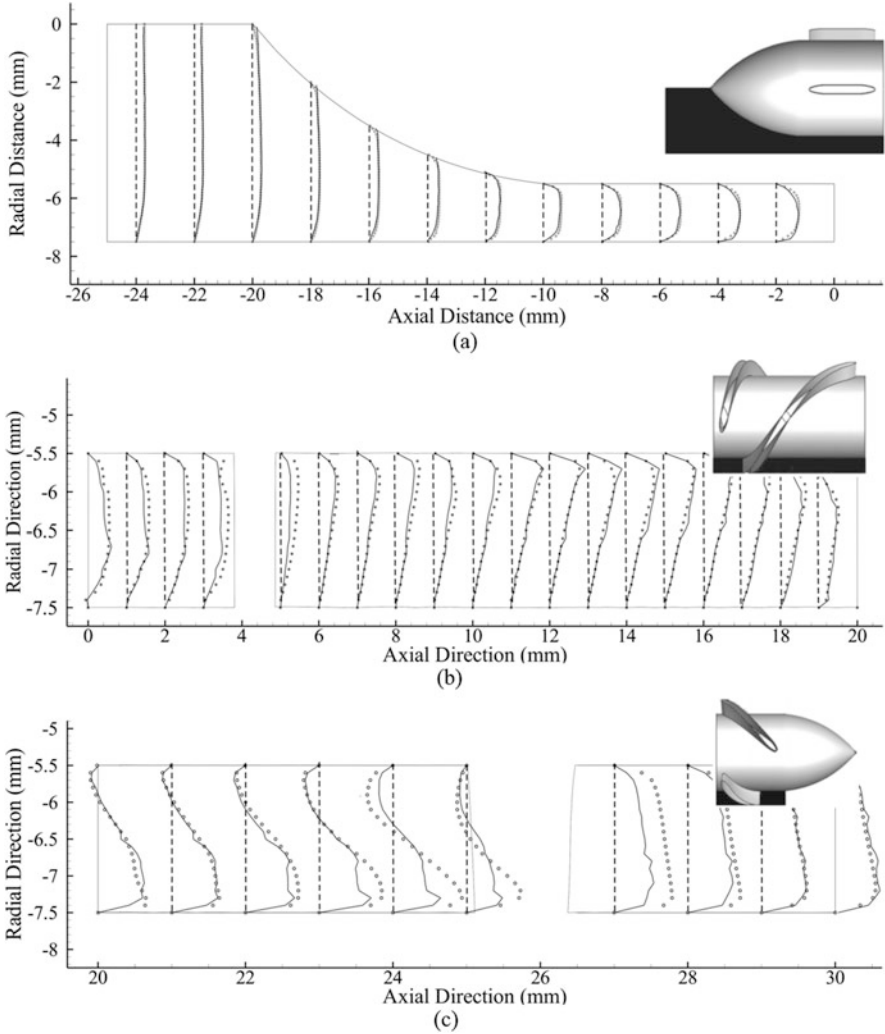


**Fig. 7.8** Comparison of the velocity profile obtained from PIV (solid line) and CFD (dotted line) results in (a) straightener, (b) impeller, and (c) diffuser. The position of plane is demonstrated by black color

CFD is a powerful tool to predict detailed flow field, which has been widely validated using PIV, and various blood damage models can be easily implemented so that it facilitates the design of artificial heart by shortening the iteration. Before clinical application, animal and clinical trials are needed to examine its blood damage level and other potential issues, which are valuable for next iteration of design if needed.

## References

1. Borovetz HS, Ramasamy N, Zerbe TR, Portner PM. Evaluation of an implantable ventricular assist system for humans with chronic refractory heart failure. *ASAIO J.* 1995;41(1):42–8.
2. Goldstein D, Oz M. *Cardiac assist devices.* New York: Future Publishing Company; 2000.
3. Song X, Throckmorton AL, Untaroiu A, Patel S, Allaire PE, Wood HG, Olsen DB. Axial flow blood pumps. *ASAIO J.* 2003;49(4):355–64.
4. Wesolowski SA, Fisher JH, Welch CS. Perfusion of the pulmonary circulation by nonpulsatile flow. *Surgery.* 1953;33(3):370–5.
5. Wood HG, Throckmorton AL, Untarolu A, Song X, Untaroiu A, Song X. The medical physics of ventricular assist devices. *Rep Prog Phys.* 2005;68(3):545.
6. Bendowski R, Morley D, Abdelsayed S, Noon GP. Clinical update and transition to destination therapy for the micromed DeBakey VAD. In: 10th Congr Inte Soc of Rotary Blood Pumps; 2002.
7. Garatti A, Bruschi G, Colombo T, Russo C, Lanfranconi M, Milazzo F, Frigerio M, Vitali E. Clinical outcome and bridge to transplant rate of left ventricular assist device recipient patients: comparison between continuous-flow and pulsatile-flow device. *Eur J Cardiothorac Surg.* 2008;34:275–80.
8. Baba A, Dobsak P, Mochizuki S, Saito I, Isoyama T, Shibata L, Takiuraand M, Abe Y, Chinzei T, Vasku J, Imachi K. Evaluation of pulsatile and nonpulsatile flow in microvessels of the bulbar conjunctiva in the goat with an undulation pump. *Artif Organs.* 2003;27(10):875–81.
9. Garon A, Farinas MI. Fast three-dimensional numerical hemolysis approximation. *Artif Organs.* 2004;28(11):1016–25.
10. Blackshear PL, Blackshear GL. In: Skalak R, Chien S, editors. *Handbook of Bioengineering.* New York: McGraw-Hill Inc.; 1987.
11. Paul R, Apel J, Schugner S, Shwindke P, Reul H. Shear stress related blood damage in laminar couette flow. *Artif Organs.* 2003;27:517–29.
12. Nose Y. Design and development strategy for the rotary blood pump. *Artif Organs.* 1998;22(6):438–46.
13. Hashimoto S, Maeda H, Sasada T. Effect of shear rate on clot growth at foreign surfaces. *Artif Organs.* 1985;9:345–50.
14. Wurzingler LJ, Blasberg P, Schmid-Schonbein H. Towards a concept of thrombosis in accelerated flow: rheology. *Fluid Dyn Biochem Biorheol.* 1985;22(5):437–500.
15. Arvand A, Hormes M, Reul H. A validated computational fluid dynamics model to estimate hemolysis in a rotary blood pump. *Artif Organs.* 2005;29(7):531–40.
16. ASTM. Standard practice for assessment of hemolysis in continuous flow blood pumps. *Annu Book ASTM Std.* 1997;13(1):1288–92.
17. Grigioni M, Daniele C, D'Avenio G, Barbaro V. A discussion on the threshold limit for hemolysis related to reynolds shear stress. *J Biomech.* 1999;32:1107–12.
18. Wurzingler LJ, Opitz R, Blasberg P, Schmid-Schonbein H. Platelet and coagulation parameters following millisecond exposure to laminar shear stress. *Thromb Haemost.* 1985;54(2):381–6.
19. Sallam AM, Hwang NHC. Human red blood cell hemolysis in turbulent shear flow: contribution of Reynolds shear stresses. *Biorheology.* 1984;21:783–97.
20. Triep M, Brucker C, Schroder W, Siess T. Computational fluid dynamics and digital particle image velocimetry study of the flow through an optimized micro-axial blood pump. *Artif Organs.* 2006;30(5):384–91.
21. Valgimigli M, Steendijk P, Serruys PW, Vranckx P, Boomsma F, Onderwater E, Vaina S, Ligthart JM, McFadden E, van der Ent M, de Jaegere P, Sianos G. Use of Impella Recover (R) LP 2.5 left ventricular assist device during high-risk percutaneous coronary interventions; clinical, haemodynamic and biochemical findings. *EuroIntervention.* 2006;2:91–100.
22. Fossum T, Morley D, Benkowski R. Chronic survival of calves implanted with the DeBakey ventricular assist device. *Artif Organs.* 1999;23:802–6.

23. Kozik DJ, Plunkett MD. Mechanical circulatory support. *Organogenesis*. 2011;7(1):50–63.
24. Chiu W-C, Slepian MJ, Bluestein D. Thrombus formation patterns in the HeartMate II ventricular assist device. *ASAIO J*. 2014;60(2):237–40.
25. Yu H, Janiga G, Thévenin D. Computational fluid dynamics-based design optimization method for archimedes screw blood pumps. *Artif Organs*. 2016;40(4):341–52.
26. Schüle CY, Thamsen B, Blümel B, Lommel M, Karakaya T, Paschereit CO, Affeld K, Kertzscher U. Experimental and numerical investigation of an axial rotary blood pump. *Artif Organs*. 2016;40(11):E192–202.
27. Lopes G, Bock E, Gómez L. Numerical analyses for low Reynolds flow in a ventricular assist device. *Artif Organs*. 2017;41(6):E30–40.
28. Graefe R, Henseler A, Steinseifer U. Multivariate assessment of the effect of pump design and pump gap design parameters on blood trauma. *Artif Organs*. 2016;40(6):568–76.
29. Su B, Chua LP, Zhong L. Numerical studies of an axial flow blood pump with different diffuser designs. *J Mech Med Biol*. 2013;13(3):1350029.
30. Burgreen GW, Antaki JF, Wu ZJ, Holmes AJ. Computational fluid dynamics as a development tool for rotary blood pumps. *Artif Organs*. 2001;25(5):336–40.
31. Yu H, Engel S, Janiga G, Thévenin D. A review of hemolysis prediction models for computational fluid dynamics. *Artif Organs*. 2017;41(7):603–21.
32. Bludszweit C. Model for general mechanical blood damage prediction. *Artif Organs*. 1995;19:583–9.
33. Giersiepen M, Wurzinger LJ, Opitz R, Reul H. Estimation of shear stress-related blood trauma in heart valve prostheses in vivo comparison of 25 aortic valves. *Artif Organs*. 1990;12:130–6.
34. Yano T, Sekine K, Mitoh A, Mitamura Y, Okamoto E, Kim D-W, Nishimura I, Murabayashi S, Yozu R. An estimation method of hemolysis within an axial flow blood pump by computational fluid dynamics analysis. *Artif Organs*. 2003;27(10):920–5.
35. Su B. Development of an axial flow ventricular assist device using computational fluid dynamics and particle image velocimetry measurement. PhD thesis. Mechanical Engineering (Nanyang Technological University); 2011.
36. Su B, Chua LP, Wang X. Validation of an axial flow blood pump: computational fluid dynamics results using particle image velocimetry. *Artif Organs*. 2012;36(4):359–67.